

# Stringent upper limits on pulsed radio emission during an active bursting phase of the Galactic magnetar SGRJ1935+2154

L. Lin<sup>\*1</sup>, C. F. Zhang<sup>\*2,3</sup>, P. Wang<sup>\*3</sup>, H. Gao<sup>1</sup>, X. Guan<sup>3</sup>, J. L. Han<sup>3,5</sup>, J. C. Jiang<sup>2,3</sup>, P. Jiang<sup>3</sup>, K. J. Lee<sup>4,3†</sup>, D. Li<sup>3,5‡</sup>, Y. P. Men<sup>2,3</sup>, C. C. Miao<sup>3</sup>, C. H. Niu<sup>3</sup>, J. R. Niu<sup>3</sup>, C. Sun<sup>3</sup>, B. J. Wang<sup>2,3</sup>, Z. L. Wang<sup>3</sup>, H. Xu<sup>2,3</sup>, J. L. Xu<sup>3</sup>, J. W. Xu<sup>2,3</sup>, Y. H. Yang<sup>6</sup>, Y. P. Yang<sup>7</sup>, W. Yu<sup>8</sup>, B. Zhang<sup>9§</sup>, B.-B. Zhang<sup>6,10,9</sup>, D. J. Zhou<sup>5,3</sup>, W. W. Zhu<sup>3</sup>, A. J. Castro-Tirado<sup>11,12</sup>, Z. G. Dai<sup>6,10</sup>, M. Y. Ge<sup>13</sup>, Y. D. Hu<sup>11,14</sup>, C. K. Li<sup>13</sup>, Y. Li<sup>4,15</sup>, Z. Li<sup>1</sup>, E. W. Liang<sup>16</sup>, S. M. Jia<sup>13</sup>, R. Quere<sup>17</sup>, L. Shao<sup>18</sup>, F. Y. Wang<sup>6,10</sup>, X. G. Wang<sup>16</sup>, X. F. Wu<sup>15</sup>, S. L. Xiong<sup>13</sup>, R. X. Xu<sup>2,4</sup>, Y.-S. Yang<sup>6</sup>, G. Q. Zhang<sup>6</sup>, S. N. Zhang<sup>13,3,5</sup>, T. C. Zheng<sup>16</sup>, J.-H. Zou<sup>18</sup>

<sup>1</sup>Department of Astronomy, Beijing Normal University, Beijing 100875, P.R.China

<sup>2</sup>Department of Astronomy, Peking University, Beijing 100871, P.R.China

<sup>3</sup>National Astronomical Observatories, Chinese Academy of Sciences, Beijing 100101, China

<sup>4</sup>Kavli institute for astronomy and astrophysics, Peking University, Beijing. 100871, P.R.China

<sup>5</sup>University of Chinese Academy of Sciences, Chinese Academy of Sciences, Beijing 100049, China

<sup>6</sup>School of Astronomy and Space Science, Nanjing University, Nanjing 210093, China

<sup>7</sup>South-Western Institute for Astronomy Research, Yunnan University, Kunming 650500, Yunnan, China

<sup>8</sup>Shanghai Astronomical observatory, Chinese Academy of Science, Shanghai 200030, China

<sup>9</sup>Department of Physics and Astronomy, University of Nevada, Las Vegas, NV 89154, USA

<sup>10</sup>Key Laboratory of Modern Astronomy and Astrophysics (Nanjing University), Ministry of Education, China

<sup>11</sup>Instituto de Astrofísica de Andalucía (IAA-CSIC), Glorieta de la Astronomía s/n, E-18008, Granada, Spain

<sup>12</sup>Departamento de Ingeniería de Sistemas y Automática, Escuela de Ingenierías, Universidad de Málaga, Dr. Pedro Ortiz Ramos, 29071 Málaga, Spain

<sup>13</sup>Key Laboratory of Particle Astrophysics, Institute of High Energy Physics, Chinese Academy of Sciences, Beijing 100049, China

<sup>14</sup>Universidad de Granada, Facultad de Ciencias Campus Fuentenueva S/N CP 18071 Granada, Spain

<sup>†</sup>E-mail: kjlee@pku.edu.cn, orcid.org/0000-0002-1435-0883

<sup>‡</sup>Email: dili@nao.cas.cn, orcid.org/0000-0003-3010-7661

<sup>§</sup>Email: zhang@physics.unlv.edu, orcid.org/0000-0002-9725-2524

<sup>15</sup>*Purple Mountain Observatory, Chinese Academy of Sciences, Nanjing 210023, China*

<sup>16</sup>*Guangxi Key Laboratory for Relativistic Astrophysics, School of Physical Science and Technology, Guangxi University, Nanning 530004 China;*

<sup>17</sup>*National Institute of Water and Atmospheric Research (NIWA), Lauder, New Zealand*

<sup>18</sup>*College of Physics, Hebei Normal University, Shijiazhuang 050024, China*

\*These authors contributed equally to this work

**Fast radio bursts (FRBs) are mysterious millisecond-duration radio transients observed from extragalactic distances<sup>1-3</sup>. Magnetars have been long speculated as the possible engine to power repeating bursts from FRB sources<sup>4-13</sup>, but no convincing evidence has been collected so far<sup>14</sup>. Recently, a Galactic magnetar dubbed Soft Gamma-ray Repeater (SGR) J1935+2154 entered an active phase by emitting intense soft gamma-ray bursts<sup>15</sup>. One fast radio burst with two peaks (hereafter FRB 200428) and a luminosity comparable to those of extragalactic FRBs was detected from the source<sup>16,17</sup> in association with a soft  $\gamma$ -ray / hard X-ray flare<sup>18-21</sup>. Here we report an eight-hour targeted observational campaign with the Five-hundred-meter Aperture Spherical radio Telescope (FAST) in four observing sessions, assisted by multi-wavelength (optical and hard X-rays) observations. During the third session, twenty-nine SGR bursts were detected by the *Fermi* Gamma-ray Burst Monitor (GBM). Throughout the observing period, especially during the scrutinized epochs when SGR bursts reached the Earth, no single dispersed pulsed emission was detected by FAST. This places a fluence upper limit eight orders of magnitude deeper than the fluence of FRB 200428. Our results suggest that FRB – SGR burst associations are rather rare. FRBs may be highly relativistic and geometrically beamed or may carry narrow spectra with the characteristic frequencies of the most bursts far outside the FAST band. More intriguingly, it is also possible that the physical condition to achieve coherent radiation in SGR bursts is contrived. Only under extreme conditions could an FRB be made in association with an SGR burst.**

We have been closely monitoring SGR J1935+2154 with FAST, aiming at testing whether a magnetar can make FRBs or FRB-like events during its active phase. We observe the target for eight hours in the following four sessions: (1) UTC 2020-04-15 21:54:00 to 2020-04-15 23:54:00, (2) 2020-04-26 21:06:55 to 2020-04-26 23:06:55, (3) 2020-04-27 23:55:00 to 2020-04-28 00:50:37; and (4) 2020-04-28 20:35:00 to 2020-04-28 23:35:00. We used the FAST central beam of L-band receiver with a usable 460 MHz band centered around 1.25 GHz. The system temperature was 20-25 K. During the FAST observing period, we also coordinated a multi-wavelength observational campaign in the hard X-ray band with *Insight*-HXMT and in the optical band with the BOOTES telescopes in China, Spain and New Zealand, as well as the LCOGT 1m telescope in

the US (Figure 1).

FRB 200428<sup>16,17</sup> occurred between our sessions (3) and (4), so the signal was not caught by FAST. On the other hand, during the one hour observing period in session (3), SGR J1935+2154 became very active, emitting 29 bursts in about thirty minutes (Methods). Both temporal and spectral properties of these events are similar to those of standard magnetar short bursts observed with GBM<sup>22,23</sup>. The fluence in 8 – 200 keV of these bursts fall in the range of  $1.8 \times 10^{-8} \sim 6.7 \times 10^{-6}$  erg cm<sup>-2</sup>. Some of these bursts have fluences comparable to or higher than  $(6.8 \pm 0.1) \times 10^{-7}$  erg cm<sup>-2</sup>, the 1-250 keV fluence of the burst associated with FRB 200428<sup>18</sup>. If associations of FRBs with SGR bursts are commonly expected, in view of the huge fluence ( $> 1.5$  MJy ms<sup>17</sup>) of FRB 200428, one would expect that there should be at least 29 FRBs detected in our time span.

We performed dedicated searches for FRB-like events in all four sessions, paying special attention to the third session when 29 SGR bursts were emitted. Since an MJy radio burst would saturate FAST, we searched for both dispersion signals and instrumental saturation signals. Five types of searching strategies have been applied: blind search, limited dispersion measure (DM) search, saturation search, windowed search, as well as ephemeris folding (Methods). No single burst signal consistent with the SGR J1935+2154 origin was detected down to the FAST sensitivity limit. Figure 2 shows the candidate single pulses detected as a function of time and DM for one example GBM burst (No. 10). The slope of the blue line tracks the expected delay time between the  $\gamma$ -ray arrival time and the radio arrival time at 1.25 GHz. The horizontal line denotes  $DM \simeq 333$  pc cm<sup>-3</sup> measured from the FRB-like events detected from the source<sup>16</sup>. One can see that no signal was detected at the desired time and DM. We checked all the pulse candidates one-by-one and identified them as narrow-band radio frequency interferences (RFIs). The same is true for all other 28 GBM bursts detected in the same observing session (Methods and Extended Data Figure 2). The non-detection of any burst from SGR J1935+2154 by FAST sets stringent upper limits on the fluxes of pulsed radio emission down to the multi-mJy level (upper panel of Extended Data Figure 1) and on the fluences down to 10-40 mJy ms level (lower panel of Extended Data Figure 1).

The lack of any FRB in association with any of the 29 SGR bursts poses important constraints on the physical mechanism producing observable FRBs from magnetars. We consider the following three possibilities. It is possible that more than one of these three possibilities are playing a role together causing the missing FRBs from most SGRs.

The first possibility is that all SGR bursts may be associated with FRBs, but the FRB jets are much more collimated than high-energy emission so that most of them missed Earth. Let us

assume that each FRB has a conical structure with a half opening angle defined as  $\max(1/\Gamma, \theta_j)$ , where  $\Gamma$  and  $\theta_j$  are the Lorentz factor and geometric opening angle of the FRB jets. The fact that at most 1/30 SGR bursts have a detectable FRB down to the FAST flux sensitivity (considering the detection of FRB 200428<sup>16,17</sup> associated with one SGR burst<sup>18–21</sup> and no reported detection of any other FRB associated with any other SGRs not in the FAST observing windows) suggests that the FRB beam solid angle must be at most 1/30 of that of SGR bursts. Assuming that the SGR emission is isotropic, one reaches the most conservative constraints of  $\Gamma \geq 59$  and  $\theta \leq 0.37$  rad, which should be more stringent if SGR bursts themselves are beamed (Methods). The requirement of  $\Gamma \gg 1$  is consistent with the suggestion that FRB emitters must be highly relativistic based on other theoretical arguments<sup>6,24</sup>. If beaming is the cause of the non-detection of FRBs from most SGR bursts, the true energies and luminosities of FRBs should be corrected by the small beaming factor  $f_{b,FRB}$  and are much lower than the isotropic values. For FRB 200428, the energy is  $< 10^{34}$  erg and the luminosity is  $< 3 \times 10^{36}$  erg s<sup>-1</sup> (Methods).

The second possibility is that all SGR bursts are accompanied by low-frequency bursts, but the peak frequencies of these bursts may have a range of distribution. This scenario may apply to the FRB models invoking relativistic shocks and contrived conditions to produce synchrotron maser emission<sup>25–28</sup>. In order to have at most 1/30 of SGRs producing FRBs observable by FAST, very contrived conditions are demanded. The required spectra of low-frequency bursts must be extremely narrow and the distribution of the peak frequencies of these bursts must be far from the FAST band. If the fluence discrepancy of FRB 200428 between CHIME<sup>16</sup> and STARE2<sup>17</sup> is caused by the intrinsic narrow spectrum of the FRB, then the distribution peak of the putative FRBs associated with other 29 SGR bursts should be above 30 GHz (Methods).

The final possibility is that the observed rarity of FRBs from SGR bursts is intrinsic. The extremely high brightness temperatures of FRBs demand that the radiation mechanism must be coherent<sup>10,11,24–29</sup>. It is possible and even likely that the fragile coherent condition may not always be satisfied in the SGR bursts. For this possibility, one would expect that the SGR burst associated with FRB 200428 may have some special features uncommon in most SGR bursts. Tentative evidence along this line has been collected<sup>18</sup>.

The non-detection of FRBs from 29 SGR bursts is consistent with the known rates of SGR bursts and cosmological FRBs. If all SGR bursts similar to the one associated with FRB 200428 generate FRBs with luminosities similar to that of FRB 200428, the cosmological FRB rate would be about two orders of magnitude higher than the currently observed value (Methods). This discrepancy is fully consistent with our observation that shows that at most 1/30 SGR bursts produce observable FRBs.

The multi-wavelength observations all set upper limits in their respective observing windows (Methods). Most of these upper limits are not constraining, but one  $Z$ -equivalent 17.9 magnitude upper limit in 60s-exposure during the prompt epoch of FRB 200428 set by BOOTES-3 can pose some interesting constraints on the models for the so-called “fast optical bursts” (FOBs) associated with FRBs<sup>30</sup>. In particular, this upper limit can rule out certain parameter space of some FOB models invoking the inverse Compton scattering origin of optical emission (Methods).

1. Lorimer, D. R., Bailes, M., McLaughlin, M. A., Narkevic, D. J. & Crawford, F. A Bright Millisecond Radio Burst of Extragalactic Origin. Science **318**, 777 (2007).
2. Petroff, E., Hessels, J. W. T. & Lorimer, D. R. Fast radio bursts. Astronomy and Astrophysics Reviews **27**, 4 (2019).
3. Cordes, J. M. & Chatterjee, S. Fast Radio Bursts: An Extragalactic Enigma. Ann. Rev. Astron. Astrophys. **57**, 417–465 (2019).
4. Popov, S. B. & Postnov, K. A. Hyperflares of SGRs as an engine for millisecond extragalactic radio bursts. In Harutyunian, H. A., Mickaelian, A. M. & Terzian, Y. (eds.) Evolution of Cosmic Objects through their Physical Activity, 129–132 (2010). 0710.2006.
5. Kulkarni, S. R., Ofek, E. O., Neill, J. D., Zheng, Z. & Juric, M. Giant Sparks at Cosmological Distances? Astrophys. J. **797**, 70 (2014).
6. Murase, K., Kashiyama, K. & Mészáros, P. A burst in a wind bubble and the impact on baryonic ejecta: high-energy gamma-ray flashes and afterglows from fast radio bursts and pulsar-driven supernova remnants. Mon. Not. R. Astron. Soc. **461**, 1498–1511 (2016).
7. Katz, J. I. How Soft Gamma Repeaters Might Make Fast Radio Bursts. Astrophys. J. **826**, 226 (2016).
8. Metzger, B. D., Berger, E. & Margalit, B. Millisecond Magnetar Birth Connects FRB 121102 to Superluminous Supernovae and Long-duration Gamma-Ray Bursts. Astrophys. J. **841**, 14 (2017).
9. Beloborodov, A. M. A Flaring Magnetar in FRB 121102? Astrophys. J. **843**, L26 (2017).
10. Kumar, P., Lu, W. & Bhattacharya, M. Fast radio burst source properties and curvature radiation model. Mon. Not. R. Astron. Soc. **468**, 2726–2739 (2017).

11. Yang, Y.-P. & Zhang, B. Bunching Coherent Curvature Radiation in Three-dimensional Magnetic Field Geometry: Application to Pulsars and Fast Radio Bursts. *Astrophys. J.* **868**, 31 (2018).
12. Wadiasingh, Z. et al. The Fast Radio Burst Luminosity Function and Death Line in the Low-twist Magnetar Model. *Astrophys. J.* **891**, 82 (2020).
13. Cheng, Y., Zhang, G. Q. & Wang, F. Y. Statistical properties of magnetar bursts and FRB 121102. *Mon. Not. R. Astron. Soc.* **491**, 1498–1505 (2020).
14. Sun, S., Yu, W., Yu, Y., Mao, D. & Lin, J. A Search for Short-term Hard X-Ray Bursts in the Direction of the Repeating FRB 121102. *Astrophys. J.* **885**, 55 (2019).
15. Veres, P., Bissaldi, E., Briggs, M. S. & Fermi GBM Team. SGR 1935+2154: Fermi GBM observation. *GRB Coordinates Network* **27531**, 1 (2020).
16. CHIME/FRB Collaboration. A bright millisecond-duration radio burst from a Galactic magnetar. arXiv e-prints arXiv:2005.10324 (2020).
17. Bochenek, C. et al. A fast radio burst associated with a Galactic magnetar. arXiv e-prints arXiv:2005.10828 (2020).
18. Zhang, S. N. et al. Insight-HXMT detection of a bright short x-ray counterpart of the Fast Radio Burst from SGR 1935+2154. *The Astronomer's Telegram* **13687**, 1 (2020).
19. Mereghetti, S. et al. SGR 1935+2154: INTEGRAL hard X-ray counterpart of radio burst. *GRB Coordinates Network* **27668**, 1 (2020).
20. Tavani, M. et al. AGILE detection of a hard X-ray burst in temporal coincidence with a radio burst from SGR 1935+2154. *The Astronomer's Telegram* **13686**, 1 (2020).
21. Ridnaia, A. et al. Konus-Wind observation of hard X-ray counterpart of the radio burst from SGR 1935+2154. *GRB Coordinates Network* **27669**, 1 (2020).
22. Collazzi, A. C. et al. The Five Year Fermi/GBM Magnetar Burst Catalog. *Astrophys. J.* **218**, 11 (2015).
23. Lin, L. et al. Burst Properties of the Most Recurring Transient Magnetar SGR J1935+2154. *Astrophys. J.* **893**, 156 (2020).
24. Lu, W. & Kumar, P. On the radiation mechanism of repeating fast radio bursts. *Mon. Not. R. Astron. Soc.* **477**, 2470–2493 (2018).

25. Lyubarsky, Y. A model for fast extragalactic radio bursts. Mon. Not. R. Astron. Soc. **442**, L9–L13 (2014).
26. Waxman, E. On the Origin of Fast Radio Bursts (FRBs). Astrophys. J. **842**, 34 (2017).
27. Metzger, B. D., Margalit, B. & Sironi, L. Fast radio bursts as synchrotron maser emission from decelerating relativistic blast waves. Mon. Not. R. Astron. Soc. **485**, 4091–4106 (2019).
28. Beloborodov, A. M. Blast Waves from Magnetar Flares and Fast Radio Bursts. arXiv e-prints (2019).
29. Katz, J. I. Coherent emission in fast radio bursts. Phys. Rev. D. **89**, 103009 (2014).
30. Yang, Y.-P., Zhang, B. & Wei, J.-Y. How Bright Are Fast Optical Bursts Associated With Fast Radio Bursts? Astrophys. J. **878**, 89 (2019).

**Acknowledgements** This work made use of data from the FAST. FAST is a Chinese national mega-science facility, built and operated by the National Astronomical Observatories, Chinese Academy of Sciences. We acknowledge the use of public data from the Fermi Science Support Center (FSSC). This work is supported by the Natural Science Foundation of China (No. 11988101, 11673002, 11703002, 11543004, 11722324, 11690024, 11633001, 11920101003, 11833003, 11722324, 11633001, 11690024, 11573014, 111725314, 11690024, 11743002, 11873067, 11533003, 11673006, U1938201, U15311243, U1831207, U1838201, U1838202, U1838113, U1938109), National Key Research and Development Programs of China (NO. 2018YFA0404204, 2017YFA0402600), the Program for Innovative Talents and Entrepreneur in Jiangsu and the KIAA-CAS Fellowship and the China Postdoctoral Science Foundation (No. 2018M631242). 2016YFA0400800, 2018YFA0400802, E01S11BQ10, XDB23010200, XDB2304040, QYZDY-SSW-SLH008, Cultivation Project for FAST Scientific Payoff and Research Achievement of CAMS-CAS, the Max-Planck Partner Group, the Spanish Science Ministry “Centro de Excelencia Severo Ochoa” Program under grant SEV-2017-0709, and the Junta de Andalucía (Project P07-TIC-03094) and support from the Spanish Ministry Projects AYA2012-39727-C03-01, AYA2015-71718R and PID2019-109974RB-I00. We thank E. Fernández-García (IAA-CSIC), I. M. Carrasco-García and C. Pérez del Pulgar (UMA) and the rest of the BOOTES Team members for making the reported BOOTES Network observations possible.

**Author Contributions** LL, BZ, and DL launched the FAST observational campaign on SGR J1935+2154; CFZ and PW systematically processed the FAST data independently and cross compared the results; KJL and DL coordinated FAST data analysis campaign; JLH, YPM, CCM, CHN, JRN, BJW, HX, JLX, WY, DJZ, and WWZ participated in the FAST data analysis. XG, PJ, CS, and ZLW coordinated FAST observations; BBZ, LL, YHY, LS, YSY, JHZ, FYW, and GQZ processed *Fermi*/GBM data; LL, SNZ, MYG, SMJ, CKL, and SLX performed joint *Insight*-HXMT observations with FAST and processed the data; BBZ, AJC-T, YDH, and RQ carried out the BOOTES optical observations; XGW, EWL, and TCZ carried out

the LCOGT optical observations; BZ coordinated the science team; HG, YPY, ZGD, YL, ZL, FYW, XFW, RXX contributed to theoretical investigations of the physical implications of the observational results. BZ, KJL, BBZ, YPY, HG, LL, CFZ, YL, and JLH contributed to the writing of the paper.

**Competing Interests** The authors declare that they have no competing financial interests.

**Correspondence** Correspondence and requests for materials should be addressed to K. J. Lee (kjlee@pku.edu.cn), D. Li (dili@naoc.ac.cn), and B. Zhang (zhang@physics.unlv.edu).



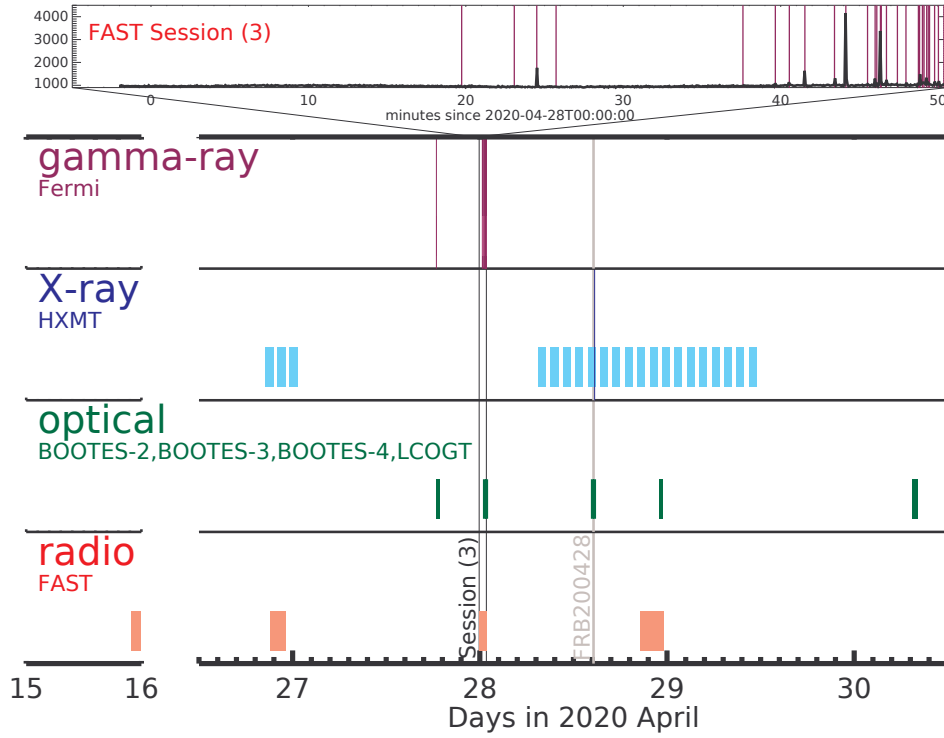


Figure 1: The timeline of our multi-wavelength observational campaign of SGR J1935+2154. From top to bottom are  $\gamma$ -rays (purple), X-rays (blue), optical (green) and radio (red). The  $\gamma$ -ray bars are the epochs of *Fermi*/GBM bursts. The bars in other bands are the observing epochs. The third FAST session during which 29 SGR bursts were detected is marked by two vertical lines, with a zoom-in timeline on the top showing the detections of 29 SGR bursts by GBM. The epoch of FRB 200428 is marked as a grey line, which coincides with one of BOOTES optical observing epochs. The second and third optical observations are artificially thickened in order to be seen more clearly.

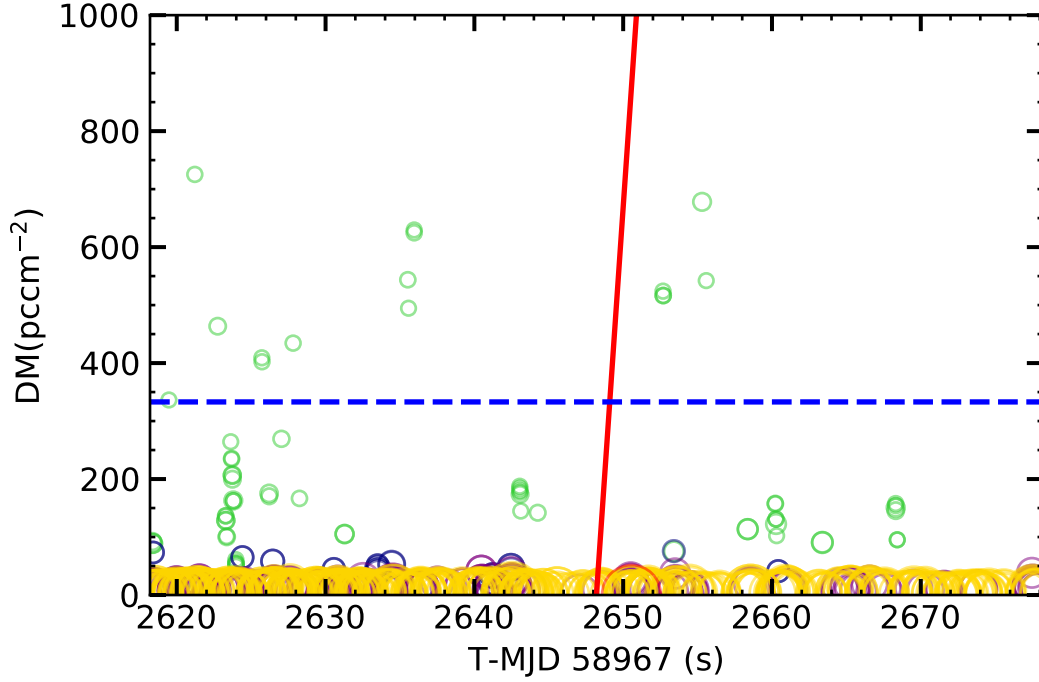


Figure 2: Non-detection of radio burst within  $\pm 30$ s of the GBM burst No. 10 around  $DM \simeq 333 \text{ pc cm}^{-3}$ . The horizontal axis is the time in seconds referring to MJD 58967. The vertical axis is the DM of the radio burst candidates. The size and color indicate the flux density of the signal, i.e. green:  $\text{flux} < 5 \text{ mJy}$ , blue  $5 \text{ mJy} < \text{flux} \leq 10 \text{ mJy}$ , purple:  $10 \text{ mJy} < \text{flux} \leq 20 \text{ mJy}$ , yellow:  $20 \text{ mJy} < \text{flux} \leq 40 \text{ mJy}$ , red:  $40 \text{ mJy} < \text{flux}$ . There is no signal with apparent flux density higher than 80 mJy. The slanted red line is the expected arrival time of a putative FRB associated with the SGR burst and the horizontal dashed blue line is the  $DM = 333 \text{ pc cm}^{-3}$  line for SGR J1935+2154. The plot is zoomed into the DM range from 0 to 1000  $\text{pc cm}^{-3}$ . The searched DM range is from 0 to 5000  $\text{pc cm}^{-3}$ .

## Methods

**Multi-wavelength campaign** The information of our multi-wavelength observational campaign is presented in Extended Data Table 1. Figure 1 shows how the multi-wavelength observations overlap in time.

**FAST observations** We performed four sessions of FAST observation as listed in Table 1: The center frequency is 1.25 GHz, spanning from 1.0 GHz to 1.5 GHz including 20 MHz band edge on each side. The average system temperature was 25 K.

We searched for the radio bursts with either a dispersion signature or instrumental saturation to all the FAST data collected during the observational campaign. We searched for dispersed bursts using the software package BEAR<sup>31</sup>. Four types of searches had been performed: 1) blind search, 2) dedicated search, 3) searching for saturation, and 4) windowed search.

Blind search: We searched the DM range from 1 to 5000  $\text{pc cm}^{-3}$ . We used following scheme to de-disperse the data to save computational resource: the DM steps are 0.3, 0.5, 1.0, and 3.0  $\text{pc cm}^{-3}$  for the DM ranges of 0 – 1000, 1000 – 1835, 1835 – 3656, 3656 – 5000  $\text{pc cm}^{-3}$ , respectively. We used 14 box-car-filter-width grids, uniformly distributed in logarithmic space from 0.2 ms to 30 ms. A zero-DM matched filter<sup>31</sup> was applied to mitigate radio frequency interference (RFI) in the blind search. All the candidate plots generated were then visually inspected. We found that most of the candidates are narrow-band RFIs, and there was no burst with dispersive signature with  $S/N \geq 8$ .

Dedicated search: For DM range of 200 to 600  $\text{pc cm}^{-3}$ , we performed a dedicated search. The DM step is refined to 0.3  $\text{pc cm}^{-3}$ . In the dedicated search, we shut down the RFI mitigator to make sure we do not throw signal away. We got no detection for wideband dispersive burst with  $S/N \geq 8$ . The DM-time plots close to 29 bursts seen in the *Fermi*/GBM daily TTE data are in Extended Data Figure 2.

Searching for saturation: We understand that if the radio flux is as high as kJy or MJy<sup>16,17</sup>, the FAST telescope would be saturated. We therefore also tried to search for saturation signals in the data. We looked for the epoch where 50% of channel satisfy one of the following conditions: 1) channel is saturated (255 value in 8bit), 2) channel is zero-valued, or 3) RMS of bandpass is less than 1. Because the DM for SGR J1935+2154 is about<sup>16,17</sup> 333  $\text{pc cm}^{-3}$ , we expect that the timescale for saturation is  $\sim 800$  ms across the FAST band. Our code captured several short timescale wide-band saturation signals. However, we did not detect any saturation lasting longer than  $> 0.5$ s. We excluded any saturation associated with SGR J1935+2145.

Windowed search: The blind search through the *Fermi*/GBM daily TTE data during the

FAST observing time revealed 37 short SGR-like bursts on 2020-04-28, from UTC 00:19 to 00:50 (Extended Data Table 2). For the FAST data within  $\pm 1$  min time window of these *Fermi*/GBM events, we performed a windowed search, where we eyeballed the plot of the dynamic spectra, DM-0 time series, and the dedispersed time series at  $333 \text{ pc cm}^{-3}$ . No burst or saturation consistent with being from SGR J1935+2145 was detected.

The non-detection places the following stringent upper limits on the pulsed radio emission from SGR J1935+2145. Using the telescope parameters<sup>32</sup>, for a 5 ms pulse, the estimated flux and fluence upper limits are 4.5 mJy and 22 mJy ms, respectively (see Extended Data Figure 1).

For the third session, we also folded the data using the ephemeris information of SGR J1935+2145<sup>33</sup> and the DM value reported<sup>16,17</sup>. No obvious signal was seen.

**Fermi Observations of SGR J1935+2154** We performed the blind search with the Bayesian Blocks method<sup>23</sup> using GBM's continued time-tagged event data. We found 29 bursts from SGR J1935 + 2154 during the third session of FAST observations. All these events were detected on 2020 April 28 in about thirty minutes from 00:19:44.192 to 00:50:21.969. The information of these bursts is listed in Extended Data Figure 2. Both flux and fluence are in 8 – 200 keV. The distribution of the burst durations ( $\langle T_{90} \rangle \sim 0.22$  s) and the cumulative distribution of fluence are presented in the two panels of Extended Data Figure 3. A cut-off power-law function

$$N(> S) = A \left[ \left( \frac{S}{10^{-7}} \right)^\alpha - \left( \frac{S_{\max}}{10^{-7}} \right)^\alpha \right] \quad (1)$$

is used to fit the cumulative distribution of fluence. Through Markov chain Monte Carlo method, the best-fit parameters are  $\alpha = 0.38^{+0.06}_{-0.07}$  and  $S_{\max} = 1.67^{+1.06}_{-0.76} \times 10^{-5} \text{ erg cm}^{-2}$ .

**Hard X-ray observations** During FAST observing sessions (2) and (4), the *Insight*-HXMT X-ray satellite<sup>34</sup> observed SGR J1935+2154 simultaneously with all its three collimated telescopes covering the 1-250 keV energy band. No significant detection of any burst was made in our offline data analysis. Assuming a cut-off power-law spectral model with the same parameters (Neutral hydrogen column density of  $2.6 \times 10^{22} \text{ cm}^{-2}$ , photon index of 1.44, and cut-off energy of 69.8 keV) as for the hard X-ray burst detected by *Insight*-HXMT in association with FRB 200428<sup>18</sup> from SGR J1935+2124, we obtained the  $3\sigma$  upper limit on its fluence as  $F_i = A_i 10^{-9} T^{-1/2} \text{ erg cm}^{-2}$ , where  $T$  is the assumed burst duration in units of second,  $i = 1, 2, 3$  represent the three telescopes, namely, LE (1-10 keV), ME (10-30 keV) and HE (27- 250 keV), and  $A_1 = 2.7$ ,  $A_2 = 3.5$  and  $A_3 = 4.5$ , respectively. With a  $T = 0.5 \text{ s}$  duration as for the X-ray burst associated with FRB 200428, its upper limits are  $3.8 \times 10^{-9} \text{ erg cm}^{-2}$ ,  $4.9 \times 10^{-9} \text{ erg cm}^{-2}$  and  $6.4 \times 10^{-9} \text{ erg cm}^{-2}$  for LE, ME and HE, respectively.

**Optical observations** We used the Burst Observer and Optical Transient Exploring System (BOOTES)<sup>35</sup> robotic telescopes and the 1-m telescope of the Las Cumbres Observatory Global Telescope (LCOGT) at McDonald Observatory to monitor SGR J1935+2154 during our FAST monitoring campaign.

The three BOOTES telescopes (0.6m BOOTES-4/MET robotic telescope at Lijiang Astronomical Observatory, China, the 60cm BOOTES-2/TELMA robotic telescope at IHSM La Mayora (UMA-CSIC) in Algarrobo Costa, Spain, and BOOTES-3 at NIWA Lauder, Otago, New Zealand) reacted various SGR alerts. They performed automatic observations on SGR J1935+2154 around the epochs of the FAST monitoring campaign. These observations lead to various  $3\sigma$  limiting magnitudes making use of the nearby stars in the USNO-B1.0 and Pan-STARRS catalog. The results are shown in Extended Data Table 1. Interestingly, a 17.9-magnitude upper limit was placed with 60-second exposure time during the epoch when FRB 200428 was emitted.

The 1-m telescope of the Las Cumbres Observatory Global Telescope (LCOGT) at McDonald Observatory took images in the  $R$  filter with an  $8 \times 300 \text{ s}$  exposure, on April 30 at 07:21:48 UT, and an upper limit 21.1 magnitude was derived from the co-added image (Extended Data Table 1).

**Constraints on model parameters: I. Beaming** The fact that 29 SGR bursts monitored by FAST did not have any associated radio burst down to the FAST sensitivity level, along with the fact that FRB 200428<sup>16,17</sup> was associated with one SGR flare<sup>18-21</sup> suggest that the probability of detecting an FRB from an SGR burst is

$$P \leq P_0 = 1/30. \quad (2)$$

---

<sup>0</sup><http://bootes.iaa.es>

The  $\leq$  sign reflects the fact that no other FRB was reported to be associated with any other SGR bursts from SGR J1935+2154. The flux contrast of these non-detections should be

$$\frac{F_{\nu,\text{FRB}}}{F_{\nu,\text{FAST}}} = \frac{f_{\nu,\text{FRB}}}{f_{\nu,\text{FAST}}} \gtrsim \eta \equiv 10^8, \quad (3)$$

where  $f_{\nu,\text{FRB}} \gtrsim 1.5 \text{ MJy ms}$  is the fluence of FRB 200428,  $f_{\nu,\text{FAST}} \sim 22 \text{ mJy ms}$  is the FAST fluence limit,  $F_{\nu,\text{FRB}}$  and  $F_{\nu,\text{FAST}}$  are the corresponding fluxes.

We consider the model constraints assuming that this small fraction is caused by the narrow beaming of FRB jets. Consider an FRB jet with a geometric beaming angle  $\theta_j$  and bulk Lorentz factor  $\Gamma$ . The Doppler factor at a viewing direction  $\theta$  is given by

$$D(\theta) = \begin{cases} 2\Gamma, & \text{for } \theta < \theta_j, \\ 1/\Gamma[1 - \beta \cos(\theta - \theta_j)], & \text{for } \theta > \theta_j. \end{cases} \quad (4)$$

For simplicity, we assume that the intrinsic spectrum of the FRB is flat, which means that the radio flux is independent of frequency (the case of a narrow spectrum is discussed below). Further we assume that FRB 200428 has  $\theta < \theta_j$  and the putative SGR-related FRBs not detected by FAST have  $\theta > \theta_j$ . One then has

$$\frac{F_{\nu}(\theta < \theta_j)}{F_{\nu}(\theta > \theta_j)} \simeq \left( \frac{D(\theta < \theta_j)}{D(\theta > \theta_j)} \right)^3 = [2\Gamma^2(1 - \beta \cos(\theta - \theta_j))]^3 \gtrsim \eta \quad (5)$$

or  $2\Gamma^2(1 - \beta \cos(\theta - \theta_j)) \gtrsim \eta^{1/3}$ . Assuming that  $|\theta - \theta_j| \ll 1$ , one has  $1 - \beta \cos(\theta - \theta_j) = 1 - \beta + \beta(\theta - \theta_j)^2/2 = 1/2\Gamma^2 + (\theta - \theta_j)^2/2$ , so that  $(\theta - \theta_j)^2\Gamma^2 \gtrsim \eta^{1/3}$ . The characteristic viewing angle above which the condition is satisfied is  $\theta_c \gtrsim \theta_j + \eta^{1/6}/\Gamma$ . If one assumes that the SGR burst emission is isotropic, the probability for FRB/SGR associations should satisfy

$$P_0 \geq P \simeq \frac{1}{4\pi} \left( 2\pi \int_0^{\theta_j + \eta^{1/6}/\Gamma} \sin \theta d\theta \right) = \frac{1}{2} \left[ 1 - \cos \left( \theta_j + \frac{\eta^{1/6}}{\Gamma} \right) \right], \quad (6)$$

which gives

$$\theta_j \leq \arccos(1 - 2P_0) - \frac{\eta^{1/6}}{\Gamma}. \quad (7)$$

In the left panel of Extended Data Figure 4, we plot the constraint from Eq.(7). For  $P_0 = 1/30$ , a small beaming angle of  $\theta_j \sim 0$  means that  $\Gamma \gtrsim \eta^{1/6}/\arccos(1 - 2P_0) \simeq 59$ , and a large Lorentz factor of  $\Gamma \gg \eta^{1/6}$  means  $\theta \lesssim \arccos(1 - 2P_0) \simeq 0.37 \text{ rad}$ . In the right panel of Extended Data Figure 4, we plot the function of  $P(\theta_j, \Gamma)$  given by Eq.(6). Such a constraint is very conservative. If the SGR bursts are not isotropic (with a beaming factor  $f_{\text{b,SGR}} < 1$ , then the constrained FRB jet angle would be smaller by the same factor.

This beaming interpretation, if true, would greatly reduce the required energetics of FRBs. The distance of SGR J1935+2154 is uncertain, ranging from  $\sim 6.6$  kpc<sup>36</sup> to  $\sim 12.5$  kpc<sup>37</sup>. We adopt the larger value to derive the most conservative upper limits on the true energetics of FRB 200428. According to the STARE2 observation, the isotropic energy of FRB 200428 is  $E_{\text{iso,FRB}} = 4\pi d^2 \nu f_{\nu,\text{FRB}} \sim 4 \times 10^{35}$  erg with  $\nu \simeq 1.4$  GHz and  $d \simeq 12.5$  kpc. If FRB 200428 as detected by STARE2 burst has the same duration as the one detected by CHIME, i.e.,  $\Delta t \sim 5$  ms, its isotropic luminosity would be  $L_{\text{iso,FRB}} \sim 8 \times 10^{37}$  erg s<sup>-1</sup>. The beaming factor of each FRB should be  $f_{\text{b,FRB}} = P f_{\text{b,SGR}} < 1/30$ . The true energy and true luminosity of FRB 200428 are therefore  $E_{\text{FRB}} \simeq E_{\text{iso,FRB}} f_{\text{b,FRB}} < 10^{34}$  erg and  $L_{\text{FRB}} < L_{\text{iso,FRB}} f_{\text{b,FRB}} < 3 \times 10^{36}$  erg s<sup>-1</sup>.

**Constraints on model parameters: II. Narrow spectra and spectral peak distribution** The small  $P \leq P_0 = 1/30$  could be also caused by narrow spectra of the putative FRBs, whose peak frequency has a distribution. Below we constrain the parameter space of this scenario.

Let us assume that every SGR burst is associated with an FRB-like burst whose peak frequency could be outside the FAST band. If the fluence of an FRB reached  $f_{\text{FAST}} \simeq 22$  mJy ms in the frequency band ( $\sim (1 - 1.5)$  GHz), it would be detected by FAST. We consider that the FRB peak frequency satisfies a log-normal distribution, i.e.

$$\frac{dN_{\text{FRB}}}{d \log \nu_{\text{peak}}} = \frac{1}{\sqrt{2\pi}\sigma_{\text{peak}}} \exp \left( -\frac{(\log \nu_{\text{peak}} - \log \bar{\nu}_{\text{peak}})^2}{2\sigma_{\text{peak}}^2} \right), \quad (8)$$

where the standard deviation is adopted as  $\sigma_{\text{peak}} = 0.5$ . For each FRB-like event, we assume that the spectrum a narrow Gaussian, i.e.

$$f_{\nu} = f_{\nu,\text{peak}} \exp \left( -\frac{(\nu - \nu_{\text{peak}})^2}{2\Delta\nu^2} \right). \quad (9)$$

The non-detection by FAST then implies

$$\eta \equiv \frac{f_{\nu,\text{FRB}}}{f_{\nu,\text{FAST}}} \simeq \frac{f_{\nu,\text{peak}}}{f_{\nu,\text{FAST}}} \lesssim \exp \left( \frac{(\nu - \nu_{\text{peak}})^2}{2\Delta\nu^2} \right), \quad (10)$$

or

$$|\nu - \nu_{\text{peak}}| \gtrsim (2 \ln \eta)^{1/2} \Delta\nu. \quad (11)$$

Therefore, the chance probability for non-detection is given by

$$P_0 \geq P \simeq \int_{\log(\max(1 \text{ GHz} - (2 \ln \eta)^{1/2} \Delta\nu, 0))}^{\log(1.5 \text{ GHz} + (2 \ln \eta)^{1/2} \Delta\nu)} \frac{dN_{\text{FRB}}}{d \log \nu_{\text{peak}}} d \log \nu_{\text{peak}}. \quad (12)$$

In the left panel of Extended Data Figure 5, we plot the relation between  $\bar{\nu}_{\text{peak}}$  and  $\Delta\nu$  constrained by the observed probability. One can see that in order to have  $P \leq P_0 = 1/30$ , the spectra should be very narrow (e.g.  $\Delta\nu < 0.1$  GHz) and the distribution peak  $\bar{\nu}_{\text{peak}}$  should be far away from the FAST band, e.g. either  $\bar{\nu}_{\text{peak}} \gtrsim (10 - 100)\text{GHz}$  or  $\bar{\nu}_{\text{peak}} \lesssim (10 - 100)\text{MHz}$ . In the right panel of Extended Data Figure 5, we show the contours for different probabilities in the  $\log \bar{\nu}_{\text{peak}} - \Delta\nu$  plane.

One may use the observation of FRB 200428 to estimate its spectral width. Given  $f_{\nu, \text{STARE2}} \sim 1.5 \text{ MJy ms}$  at  $\nu_{\text{STARE2}} \sim 1.4 \text{ GHz}$  and  $f_{\nu, \text{CHIME}} \sim 0.22 \text{ MJy ms}$  at  $\nu_{\text{CHIME}} \sim 0.6 \text{ GHz}$ , one can use

$$\frac{f_{\nu, \text{STARE2}}}{f_{\nu, \text{CHIME}}} = \exp\left(\frac{(\nu_{\text{CHIME}} - \nu_{\text{STARE2}})^2}{2\Delta\nu^2}\right) \quad (13)$$

to derive

$$\Delta\nu = \frac{|\nu_{\text{CHIME}} - \nu_{\text{STARE2}}|}{[2(\ln f_{\nu, \text{STARE2}} - \ln f_{\nu, \text{CHIME}})]^{1/2}} \sim 0.4 \text{ GHz}. \quad (14)$$

As shown in Extended Data Figure 5 left panel, this requires that the peak of  $\nu_{\text{peak}}$  distribution is far away from the FAST band, i.e.  $\bar{\nu}_{\text{peak}} \geq 32 \text{ GHz}$ .

**Constraints on the fraction of SGRs bursts that produce FRBs** In the following, we show that in order not to overproduce the observed FRB rate in the universe, only a small fraction of SGR bursts are allowed to make detectable FRBs.

We first estimate the cosmic number density of SGRs as

$$\mathcal{F}(z) = f_{\text{NS}} \cdot f_{\text{SGR}} \cdot \int_{\infty}^z \dot{\rho}(z') \cdot \frac{d\tau_{z'}}{dz'} dz', \quad (15)$$

where  $\dot{\rho}(z)$  is the star formation rate as a function of redshift  $z$ ,  $\tau_z$  is the age of the universe at redshift  $z$ ,  $f_{\text{NS}}$  represents the specific neutron star formation fraction per  $M_{\odot}$ , and  $f_{\text{SGR}}$  denotes the fraction of NSs that can produce SGR bursts (magnetars). We adopt the analytical model of the star formation history derived from the observational data<sup>38</sup>

$$\dot{\rho}(z) = \dot{\rho}_0 \left[ (1+z)^{3.4\eta} + \left(\frac{1+z}{5000}\right)^{-0.3\eta} + \left(\frac{1+z}{9}\right)^{-3.5\eta} \right]^{\frac{1}{\eta}}, \quad (16)$$

where  $\dot{\rho}_0 = 0.02 M_{\odot} \text{yr}^{-1} \text{Mpc}^{-3}$ , and the smoothing parameter  $\eta = -10$ . The age of the universe for the standard  $\Lambda\text{CDM}$  cosmology is defined as

$$\tau_z = \frac{1}{H_0} \int_z^{\infty} \frac{dz'}{(1+z')[\Omega_M(1+z')^3 + \Omega_{\Lambda}]^{1/2}}, \quad (17)$$



where Planck cosmological parameters, i.e.  $H_0 = 67.8 \text{ km s}^{-1} \text{ Mpc}^{-1}$ ,  $\Omega_m = 0.308$ , and  $\Omega_\Lambda = 0.692$  have been adopted<sup>39</sup>. Assuming that all formed stars obey the Salpeter initial mass function<sup>40</sup>  $dN/dM \propto M^{-2.35}$  within the mass range  $0.1 - 100 M_\odot$  and that the massive stars with  $8 M_\odot < M < 25 M_\odot$  would produce neutron stars within a negligible timescale compared with  $\tau_z$ , we roughly obtain  $f_{\text{NS}} = 0.006 M_\odot^{-1}$ . On the other hand, based on the Milky Way observations, we can give an order of magnitude estimation for  $f_{\text{SGR}} \sim N_{\text{SGR,obs}}/N_{\text{NS,MW}} \sim 10^{-7}$ .

In order to estimate the FRB rate, we further assume that on average SGRs produce hard X-ray/soft  $\gamma$ -ray bursts with a bursting rate  $\dot{N}_b \text{ day}^{-1}$ , where a fraction of  $f_{\text{SGR-FRB}}$  among  $\dot{N}_b$  bursts can generate FRBs observable by Earth observers. Consequently, the rate of FRBs from SGRs (SGR-FRBs hereafter) could be estimated as

$$\frac{dN_{\text{FRB}}}{dV \cdot dt} = \mathcal{F}(z) \cdot \dot{N}_b \cdot f_{\text{SGR-FRB}}. \quad (18)$$

For a given detector with the sensitivity threshold  $F_{\text{th}}$ , the threshold luminosity of detectable FRBs at redshift  $z$  is  $L_{\text{th}} = 4\pi D_L^2(z) F_{\text{th}}$ . Here we adopt  $F_{\text{th}} \sim 1 \text{ mJy}$  considering the sensitivity of CHIME<sup>41</sup>. We assume that the luminosity function of SGR-FRBs is  $dN/dL \propto L^{-\alpha}$  within the luminosity range  $L_0 < L < L_{\text{cut}}$ , where we take  $\alpha = 1.8$  and  $L_{\text{cut}} = 10^{44} \text{ erg s}^{-1}$  based on the currently known FRB luminosity function<sup>42</sup>. We assume  $L_0 = L_{\text{obs}}$ , where  $L_{\text{obs}} = 8 \times 10^{37} \text{ erg s}^{-1}$  is the luminosity of FRB 200428. We finally derive the SGR-FRB detection rate

$$\mathcal{R}_{\text{SGR-FRB}} \sim \int_0^{z_{\text{max}}} \mathcal{F}(z) \cdot \dot{N}_b \cdot f_{\text{SGR-FRB}} \cdot \left( \frac{L_{\text{th}}}{L_0} \right)^{-(\alpha-1)} \cdot \frac{dV(z)}{dz} dz, \quad (19)$$

where

$$\frac{dV(z)}{dz} = \frac{c}{H_0} \frac{4\pi D_L^2(z)}{(1+z)^2 [\Omega_M(1+z)^3 + \Omega_\Lambda]^{1/2}}, \quad (20)$$

and  $4\pi D_L^2(z_{\text{max}}) F_{\text{th}} = L_{\text{cut}}$ . Considering that  $\mathcal{R}_{\text{SGR-FRB}}$  should be smaller than the observational rate of FRBs, which is  $\sim 10^4 \text{ day}^{-1}$  all sky<sup>2</sup>, we thus obtain

$$f_{\text{SGR-FRB}} \lesssim 1.7 \times 10^{-2} \left( \frac{\mathcal{R}_{\text{SGR-FRB}}}{10^4 \text{ day}^{-1}} \right) \left( \frac{f_{\text{SGR}}}{10^{-7}} \right)^{-1} \left( \frac{\dot{N}_b}{10^{-4} \text{ day}^{-1}} \right)^{-1}. \quad (21)$$

This fraction is fully consistent with the fact that at most 1/30 of SGRs can produce observable FRBs.

**Model constraints from non-detection of FOB** The 17.9 mag upper limit of the optical flux during the prompt phase of FRB 200428 can be used to constrain physical models of FRBs. Consider

that the extinction correction of 6.2 mag in the direction SGR J1935+2154. The true upper limit is  $\sim 11.7$  mag.

Following Ref.<sup>30</sup>, we consider a putative “fast optical burst” (FOB) with peak flux of  $F_\nu$  and duration  $\tau$ . For a telescope with exposure time  $T$ , the observed effective flux could be estimated as  $F_{\nu,\text{eff}} \sim \min(\tau/T, 1)F_\nu$ . The magnitude of an optical source is related to its flux through  $m = -2.5 \log_{10}(F_\nu/3631 \text{ Jy})$ , one has

$$m = 20.8 - 2.5 \log_{10} \left( \frac{\tau_{\text{ms}} F_{\nu,\text{Jy}}}{T_{60}} \right) \quad (22)$$

for  $\tau \lesssim T$ , where  $\tau_{\text{ms}}$  is the optical pulse duration normalized to milliseconds,  $T_{60}$  is the exposure time normalized to 60 s, and  $F_{\nu,\text{Jy}}$  is the peak flux in Jansky. For a given observed limiting magnitude  $m_*$ , the intrinsic flux limit of an FOB would be

$$F_{\nu,\text{opt}} = \left( \frac{T_{60}}{\tau_{\text{ms}}} \right) 10^{(8.32-0.4m_*)} \text{ Jy} \quad (23)$$

for  $\tau \lesssim T$ . Our BOOTES observation gives an upper limit  $m_* = 11.7$  with  $T = 60$  s after considering the extinction correction. One then has  $F_{\nu,\text{opt}} \lesssim 4.4 \text{ kJy}$  for  $\tau = 1 \text{ ms}$ . The flux of the FRB 200428 is  $F_{\nu,\text{FRB}} \gtrsim 1.5 \text{ MJy}$  for  $\tau = 1 \text{ ms}$ . One therefore has

$$\zeta \equiv \frac{F_{\nu,\text{opt}}}{F_{\nu,\text{FRB}}} \lesssim 10^{-3}. \quad (24)$$

This stringent upper limit of  $\zeta$  starts to pose interesting constraints on FOB emission mechanisms<sup>30</sup>. For models invoking extension of radio emission to the optical band, the predicted optical flux is lower than this limit. These models are therefore consistent with the upper limit. On the other hand, some models invoking inverse Compton (IC) scattering off radio photons to the optical band can be constrained with the current limit. Let us define the fraction of electrons that can upscatter radio photons to the optical band is  $\eta_\gamma \leq 1$ . The following constraints can be made: (1) For the IC model within the magnetosphere of a neutron star,  $\zeta \lesssim 10^{-3}$  leads to the constraint  $\eta_\gamma \lesssim 3000$ . Since  $\eta_\gamma$  is supposed to be  $\leq 1$ , this scenario is fully consistent with the data. (2) For a beamed radio burst with intrinsic duration  $\Delta t$ , opening angle  $\theta_j$ , and rotation period  $P \sim 3.2 \text{ s}$  sweeping a surrounding nebula, the duration of the FOB due to IC scattering is much longer, i.e.,  $\tau \sim 1000 \text{ s}$ . The intrinsic optical flux then becomes  $F_{\nu,\text{opt}} \simeq 76 \text{ mJy}$ , so that  $\zeta \lesssim 10^{-8}$ . This gives the constraint  $\eta_\gamma \lesssim 0.5(\Delta t/1 \text{ ms})^{-1}$ , or  $\eta_\gamma \lesssim 1.7 \times 10^{-4}(\theta_j/0.1)^{-2}$ . This is the first meaningful constraint on the FOB model parameters.

31. Men, Y. P. et al. Piggyback search for fast radio bursts using Nanshan 26 m and Kunming 40 m radio telescopes - I. Observing and data analysis systems, discovery of a mysterious peryton. Mon. Not. R. Astron. Soc. **488**, 3957–3971 (2019).
32. Jiang, P. et al. The Fundamental Performance of FAST with 19-beam Receiver at L Band. arXiv e-prints arXiv:2002.01786 (2020).
33. Israel, G. L. et al. The discovery, monitoring and environment of SGR J1935+2154. Mon. Not. R. Astron. Soc. **457**, 3448–3456 (2016).
34. Zhang, S.-N. et al. Overview to the Hard X-ray Modulation Telescope (Insight-HXMT) Satellite. Science China Physics, Mechanics, and Astronomy **63**, 249502 (2020).
35. Castro-Tirado, A. J. et al. Building the BOOTES world-wide Network of Robotic telescopes. In Astronomical Society of India Conference Series, vol. 7 of Astronomical Society of India Conference Series, 313–320 (2012).
36. Zhou, P. et al. Revisiting the distance, environment and supernova properties of SNR G57.2+0.8 that hosts SGR 1935+2154. arXiv e-prints arXiv:2005.03517 (2020).
37. Kothes, R., Sun, X., Gaensler, B. & Reich, W. A Radio Continuum and Polarization Study of SNR G57.2+0.8 Associated with Magnetar SGR 1935+2154. Astrophys. J. **852**, 54 (2018).
38. Yüksel, H., Kistler, M. D., Beacom, J. F. & Hopkins, A. M. Revealing the High-Redshift Star Formation Rate with Gamma-Ray Bursts. Astrophys. J. **683**, L5 (2008).
39. Planck Collaboration et al. Planck 2015 results. XIII. Cosmological parameters. Astron. Astrophys. **594**, A13 (2016).
40. Salpeter, E. E. The Luminosity Function and Stellar Evolution. Astrophys. J. **121**, 161 (1955).
41. CHIME/FRB Collaboration et al. The CHIME Fast Radio Burst Project: System Overview. Astrophys. J. **863**, 48 (2018).
42. Luo, R. et al. On the FRB luminosity function - - II. Event rate density. Mon. Not. R. Astron. Soc. **494**, 665–679 (2020).

## Extended Data

Extended Data Table 1: **Information of multi-wavelength campaign.**

Extended Data Table 2: **The information of the 29 SGR bursts detected by *Fermi*/GBM.**

Extended Data Figure 1: **Flux and fluence upper limits from FAST observation.** The horizontal axis is the pulse width. The upper and lower panels are the flux and fluence upper limits, respectively.

Extended Data Figure 2: **FRB radio candidates around the epochs of all 29 *Fermi*/GBM bursts.** Each panel is similar to Figure 2, except that they are centered around the epochs of different GBM bursts.

Extended Data Figure 3:  **$T_{90}$  and fluence distribution of 29 *Fermi*/GBM bursts with best fitting lines.** The upper panel is the duration  $T_{90}$  distribution, and the lower panel is the fluence distribution.

Extended Data Figure 4: **Jet beaming angle constraints.** Left panel: The relation between jet beaming angle  $\theta_j$  and Lorentz factor  $\Gamma$  constrained by the observed probability, see Eq.(7). Right panel: The constrained probability ( $P$ ) contours in the  $\theta_j - \Gamma$  plane. The color scale is in logarithmic scale, i.e.,  $\log(P)$ .

Extended Data Figure 5: **Spectra and spectral peak distribution constraints.** Left panel: The relation between  $\bar{\nu}_{\text{peak}}$  and  $\Delta\nu$  constrained by the observed probability. The dashed line corresponds to  $\Delta\nu = 0.4$  GHz. Right panel: The constrained probability contour in the  $\bar{\nu}_{\text{peak}} - \Delta\nu$  plane. The color scale is in logarithmic scale, i.e.,  $\log(P)$ .

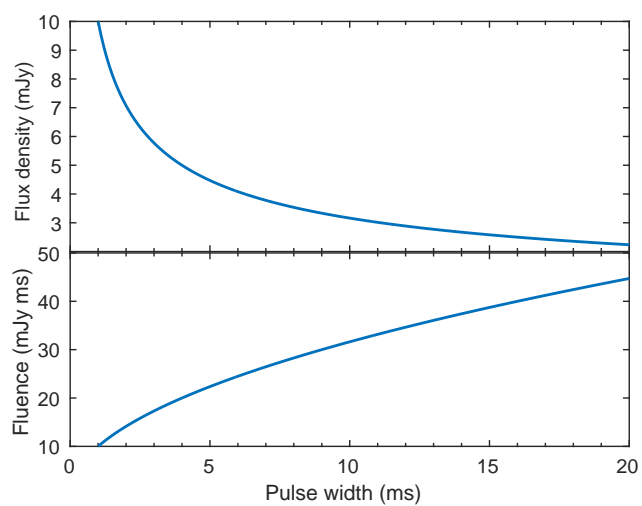
**Extended Data Table 1: Information of multi-wavelength campaign**

band	telescope	location	UTC start	UTC end	Exp (s)	limits
1.25GHz	FAST, Session (1)	Pingtang, China	2020-04-15T21:54:00	2020-04-15T23:54:00	7200	$< 22$ mJy ms
1.25GHz	FAST, Session (2)	Pingtang, China	2020-04-26T21:06:55	2020-04-26T23:06:55	7200	$< 22$ mJy ms
1.25GHz	FAST, Session (3)	Pingtang, China	2020-04-27T23:55:00	2020-04-28T00:50:37	3337	$< 22$ mJy ms
1.25GHz	FAST, Session (4)	Pingtang, China	2020-04-28T20:35:00	2020-04-28T23:35:00	10800	$< 22$ mJy ms
clear	BOOTES-4	Lijiang, China	2020-04-27T18:26:53	2020-04-27T18:56:53	$60 \times 30$	$> 20.5$ mag <sup>a</sup>
<i>Z</i>	BOOTES-2	Algarrobo Costa, Málaga, Spain	2020-04-28T00:44:03	2020-04-28T00:48:14	$5 \times 50$	$> 15.9$ mag
<i>Z</i>	BOOTES-3	NIWA Lauder, Otago, New Zealand	2020-04-28T14:34:24	2020-04-28T14:35:24	60	$> 17.9$ mag
clear	BOOTES-2	Algarrobo Costa, Málaga, Spain	2020-04-28T22:57:44	2020-04-28T23:27:44	$60 \times 30$	$> 20.4$ mag
<i>R</i>	LCOGT	Fort Davis, US	2020-04-30T07:21:49	2020-04-30T08:07:08	$8 \times 300$	$> 21.1$ mag
1 – 250 keV	Insight-HXMT	...	2020-04-26T20:14:50	2020-04-27T00:40:56	$3 \times 3675$	$< (\text{LE} : 3.8, \text{ME} : 4.9, \text{HE} : 6.4) \times 10^{-9} \text{ erg cm}^{-2}$
1 – 250 keV	Insight-HXMT	...	2020-04-28T07:27:03	2020-04-29T11:30:02	$18 \times 3738$	$< (\text{LE} : 3.8, \text{ME} : 4.9, \text{HE} : 6.4) \times 10^{-9} \text{ erg cm}^{-2}$

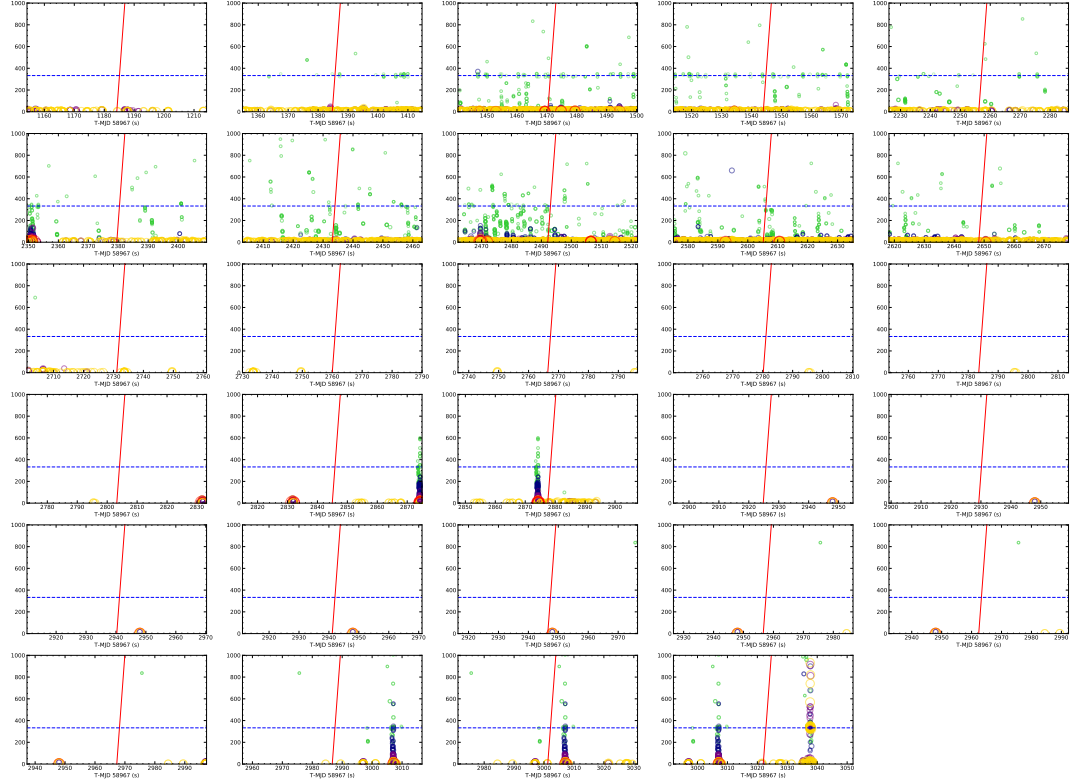
<sup>a</sup> All optical magnitude upper limits are subject to extinction correction, which is 6.2 mag in *Z* band for SGR J1935+2154.

**Extended Data Table 2: The information of the 29 SGR bursts detected by *Fermi*/GBM**

ID	Burst time	Flux (erg cm <sup>-2</sup> s <sup>-1</sup> )	Fluence (erg cm <sup>-2</sup> )
1	00:19:44.192	$1.22^{+0.18}_{-0.16} \times 10^{-6}$	$7.93^{+1.20}_{-1.05} \times 10^{-8}$
2	00:23:04.728	$3.26^{+0.73}_{-0.67} \times 10^{-7}$	$7.10^{+1.58}_{-1.47} \times 10^{-8}$
3	00:24:30.296	$2.37^{+0.05}_{-0.05} \times 10^{-5}$	$3.01^{+0.06}_{-0.07} \times 10^{-6}$
4	00:25:43.945	$1.99^{+0.70}_{-0.62} \times 10^{-7}$	$5.26^{+1.84}_{-1.64} \times 10^{-8}$
5	00:37:36.153	$2.73^{+0.58}_{-0.55} \times 10^{-7}$	$6.78^{+1.43}_{-1.35} \times 10^{-8}$
6	00:39:39.513	$8.96^{+1.09}_{-1.04} \times 10^{-7}$	$1.89^{+0.23}_{-0.22} \times 10^{-7}$
7	00:40:33.072	$1.20^{+0.11}_{-0.11} \times 10^{-6}$	$3.57^{+0.32}_{-0.33} \times 10^{-7}$
8	00:41:32.136	$4.69^{+0.16}_{-0.17} \times 10^{-6}$	$1.15^{+0.04}_{-0.04} \times 10^{-6}$
9	00:43:25.169	$2.23^{+0.14}_{-0.13} \times 10^{-6}$	$5.51^{+0.35}_{-0.33} \times 10^{-7}$
10	00:44:08.202	$3.93^{+0.08}_{-0.07} \times 10^{-5}$	$6.68^{+0.13}_{-0.13} \times 10^{-6}$
11	00:45:31.097	$8.44^{+1.32}_{-1.16} \times 10^{-7}$	$7.43^{+1.16}_{-1.02} \times 10^{-8}$
12	00:46:00.009	$7.83^{+0.66}_{-0.67} \times 10^{-7}$	$4.52^{+0.38}_{-0.39} \times 10^{-7}$
13	00:46:06.408	$4.11^{+0.64}_{-0.61} \times 10^{-7}$	$7.89^{+1.23}_{-1.17} \times 10^{-8}$
14	00:46:20.176	$2.32^{+0.06}_{-0.05} \times 10^{-5}$	$4.18^{+0.10}_{-0.09} \times 10^{-6}$
15	00:46:23.504	$3.17^{+0.46}_{-0.43} \times 10^{-7}$	$2.32^{+0.33}_{-0.31} \times 10^{-7}$
16	00:46:43.208	$9.81^{+0.75}_{-0.69} \times 10^{-7}$	$3.21^{+0.24}_{-0.23} \times 10^{-7}$
17	00:47:24.961	$1.66^{+0.43}_{-0.34} \times 10^{-7}$	$6.23^{+1.61}_{-1.29} \times 10^{-8}$
18	00:47:57.528	$1.16^{+0.12}_{-0.11} \times 10^{-6}$	$1.08^{+0.11}_{-0.10} \times 10^{-7}$
19	00:48:44.824	$3.96^{+0.46}_{-0.42} \times 10^{-7}$	$1.38^{+0.16}_{-0.15} \times 10^{-7}$
20	00:48:49.272	$3.05^{+0.17}_{-0.16} \times 10^{-6}$	$7.32^{+0.40}_{-0.38} \times 10^{-7}$
21	00:49:00.273	$7.80^{+1.14}_{-1.03} \times 10^{-7}$	$8.11^{+1.18}_{-1.07} \times 10^{-8}$
22	00:49:01.121	$8.36^{+0.96}_{-0.92} \times 10^{-7}$	$1.32^{+0.15}_{-0.14} \times 10^{-7}$
23	00:49:06.472	$9.66^{+4.00}_{-3.73} \times 10^{-8}$	$6.98^{+2.89}_{-2.69} \times 10^{-8}$
24	00:49:16.592	$1.78^{+0.16}_{-0.15} \times 10^{-7}$	$4.17^{+1.28}_{-1.24} \times 10^{-8}$
25	00:49:22.392	$7.72^{+1.10}_{-1.05} \times 10^{-7}$	$4.55^{+0.65}_{-0.62} \times 10^{-8}$
26	00:49:27.280	$3.58^{+1.32}_{-1.08} \times 10^{-7}$	$2.11^{+0.78}_{-0.64} \times 10^{-8}$
27	00:49:46.680	$3.87^{+0.39}_{-0.36} \times 10^{-7}$	$2.63^{+0.26}_{-0.24} \times 10^{-7}$
28	00:50:01.248	$7.83^{+0.66}_{-0.61} \times 10^{-7}$	$3.13^{+0.26}_{-0.25} \times 10^{-7}$
29	00:50:21.969	$1.32^{+0.55}_{-0.46} \times 10^{-7}$	$1.85^{+0.76}_{-0.65} \times 10^{-8}$

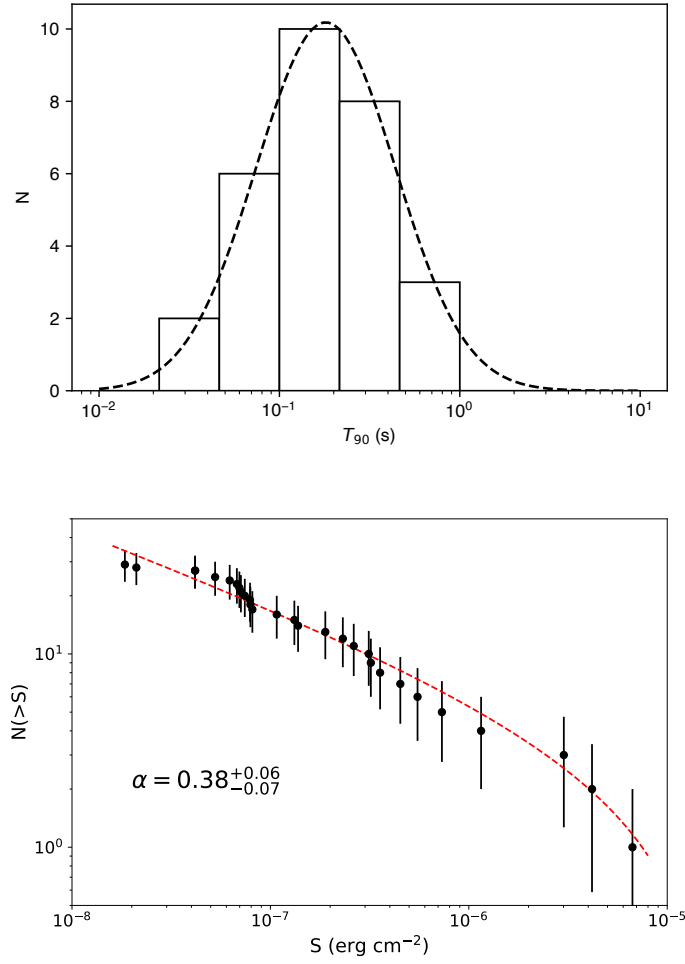


**Extended Data Figure 1: Flux and fluence upper limits from FAST observation.** The horizontal axis is the pulse width. The upper and lower panels are the flux and fluence upper limits, respectively.

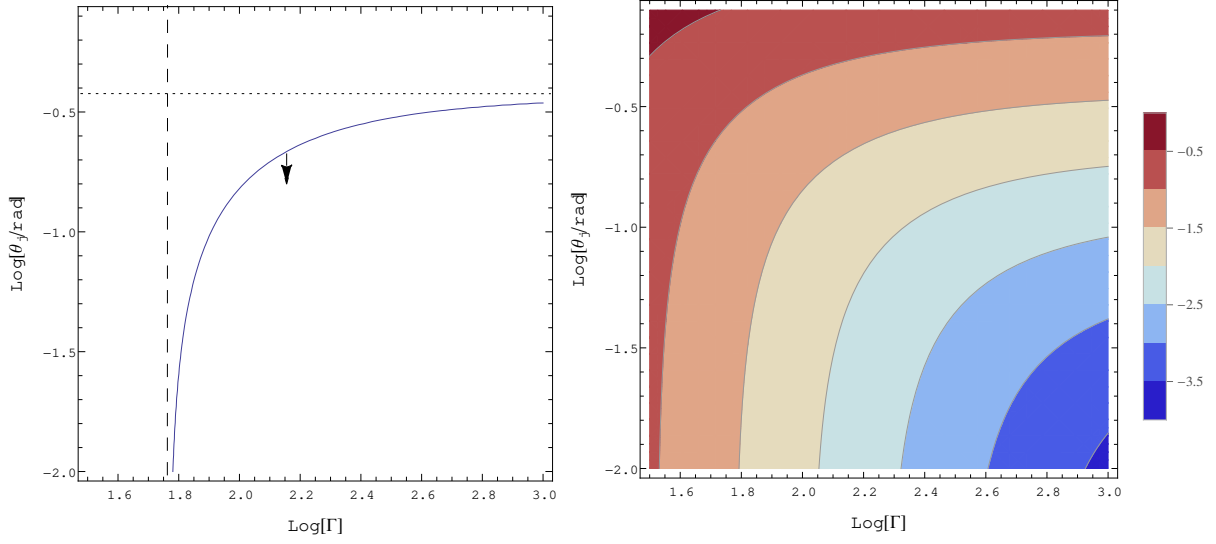


**Extended Data Figure 2: FRB radio candidates around the epochs of all 29 *Fermi*/GBM bursts.** Each panel is similar to Figure 2, except that they are centered around the epochs of different GBM bursts.

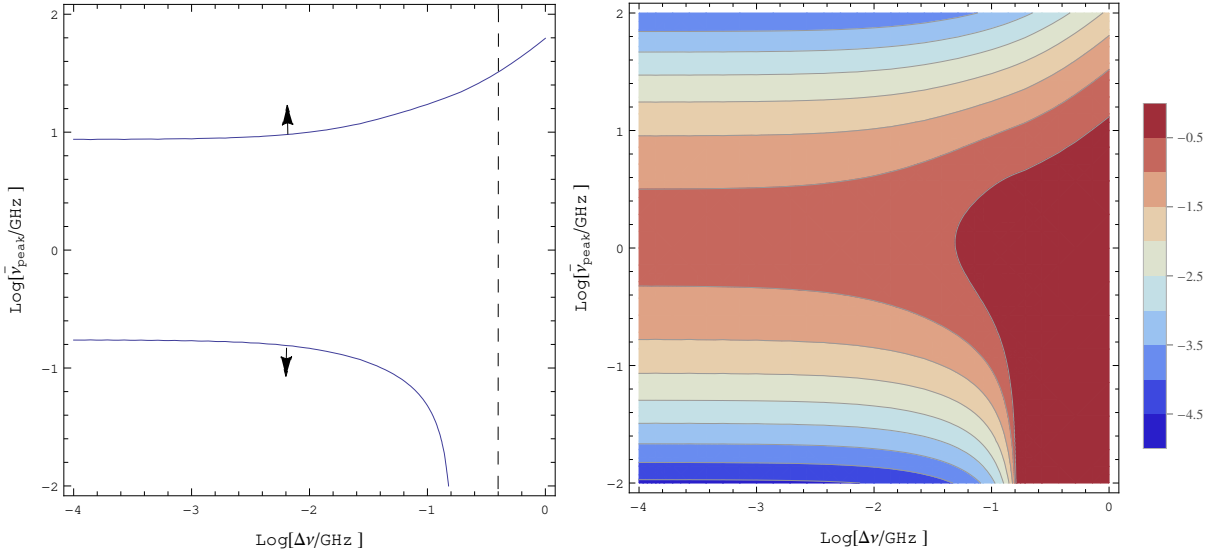




**Extended Data Figure 3:  $T_{90}$  and fluence distribution of 29 *Fermi*/GBM bursts with best fitting lines.** The upper panel is the duration  $T_{90}$  distribution, and the lower panel is the fluence distribution.



**Extended Data Figure 4: Jet beaming angle constraints.** Left panel: The relation between jet beaming angle  $\theta_j$  and Lorentz factor  $\Gamma$  constrained by the observed probability, see Eq.(7). Right panel: The constrained probability ( $P$ ) contours in the  $\theta_j - \Gamma$  plane. The color scale is in logarithmic scale, i.e.,  $\log(P)$ .



**Extended Data Figure 5: Spectra and spectral peak distribution constraints.** Left panel: The relation between  $\bar{\nu}_{\text{peak}}$  and  $\Delta\nu$  constrained by the observed probability. The dashed line corresponds to  $\Delta\nu = 0.4$  GHz. Right panel: The constrained probability contour in the  $\bar{\nu}_{\text{peak}} - \Delta\nu$  plane. The color scale is in logarithmic scale, i.e.,  $\log(P)$ .